

## Supporting Information

### Nuclearity Effects in Supported, Single-Site Fe(II) Hydrogenation Pre-Catalysts

Ryan R. Langeslay,<sup>a</sup> Hyuntae Sohn,<sup>a</sup> Bo Hu,<sup>a,b</sup> Jacob S. Mohar,<sup>a</sup> Magali Ferrandon,<sup>a</sup> Cong Liu,<sup>a</sup>  
Hacksung Kim,<sup>a,c</sup> A. Jeremy Kropf,<sup>a</sup> Ce Yang,<sup>a</sup> Jens Niklas,<sup>a</sup> Oleg G. Poluektov,<sup>a</sup> E. Ercan Alp,<sup>d</sup>  
Patricia Ignacio-de Leon,<sup>e</sup> Alfred P. Sattelberger,<sup>a\*</sup> Adam S. Hock,<sup>a,b\*</sup> and Massimiliano  
Delferro<sup>a\*</sup>

<sup>a</sup>*Chemical Sciences and Engineering Division, Argonne National Laboratory, Lemont, IL 60439, USA*

<sup>b</sup>*Department of Chemistry, Illinois Institute of Technology, Chicago IL 60616, USA*

<sup>c</sup>*Catalysis Center, Northwestern University, Evanston, IL 60208, USA*

<sup>d</sup>*X-ray Science Division, Argonne National Laboratory, Lemont, IL 60439, USA*

<sup>e</sup>*Energy Sciences Division, Argonne National Laboratory, Lemont, IL 60439, USA*

## Table of Contents

Materials and Methods.....	S3
Physical and Analytical Measurements.....	S3
EPR Analysis.....	S4
Catalyst Synthesis.....	S5
NMR Grafting Experiments.....	S6
Preparation of <sup>57</sup> Fe-labeled Catalysts.....	S6
X-ray Absorption Experiments.....	S6
Catalyst Testing.....	S7
GC-MS and GC-FID Analysis.....	S8
Computational Details.....	S13
References.....	S18

## List of Figures and Tables

<b>Table 1.</b> Observed and calculated (DFT) frequencies (cm <sup>-1</sup> ) in the Raman spectra.....	S8
<b>Figure S1.</b> DRIFTS analysis of SiO <sub>2-700</sub> , and SiO <sub>2-200</sub> .....	S9
<b>Figure S2.</b> An example NMR spectrum in Toluene-d <sub>8</sub> from the grafting experiments.....	S9
<b>Figure S3.</b> Comparison of EPR signals from FeSiO <sub>2-200</sub> , <b>2</b> , prepared at 2% Fe, 0.1% Fe, and 0.1% Fe magnified 20x.....	S10
<b>Figure S4.</b> EPR results for FeSiO <sub>2-200</sub> , <b>2</b> , prepared at 0.1% Fe, SiO <sub>2-200</sub> background, and resulting background-subtracted spectra.....	S10
<b>Figure S5.</b> EPR results for FeSiO <sub>2-700</sub> , <b>1</b> .....	S11
<b>Figure S6.</b> EPR results for FeSiO <sub>2-200</sub> , <b>2</b> .....	S11
<b>Figure S7.</b> Diffuse Reflectance Infrared Fourier Transform Spectroscopy.....	S12
<b>Figure S8.</b> Diffuse Reflectance Ultraviolet-Visible Spectra of <b>1</b> and <b>2</b> (red).....	S12
<b>Figure S9.</b> Appearance of [Fe( $\mu$ -Mes)Mes] <sub>2</sub> , <b>1</b> , and <b>2</b> .....	S13
<b>Figure S10.</b> Cluster models of (a) SiO <sub>2-200</sub> and (b) SiO <sub>2-700</sub> .....	S14
<b>Figure S11.</b> Optimized structures of <b>1</b> and <b>2</b> .....	S14
<b>Figure S12.</b> TEM images of <b>1</b> and <b>2</b> as prepared and after H <sub>2</sub> treatment.....	S15
<b>Figure S13.</b> Fe K edge XANES.....	S16
<b>Figure S14.</b> Magnitude of the k <sup>2</sup> -weighted Fourier transform from 3 Å <sup>-1</sup> < k < 8.5 Å <sup>-1</sup> .....	S17

## EXPERIMENTAL

**Materials and Methods.** Unless otherwise stated, all manipulations described below were carried out with rigorous exclusion of O<sub>2</sub> and moisture using Schlenk and glovebox techniques. Benzene-d<sub>6</sub> and toluene-d<sub>8</sub> (Sigma-Aldrich) were dried over activated alumina and degassed using three freeze-pump-thaw cycles prior to use. Solvents were purchased from Sigma-Aldrich and were sparged with nitrogen and dried over activated alumina before use. The 1,3,5-tri-tertbutyl benzene internal integration standard for NMR grafting studies was purchased from Sigma-Aldrich, sublimed under high-vacuum, and stored in the glove box. [Fe( $\mu$ -Mes)Mes]<sub>2</sub> was prepared according to a modified literature procedure<sup>1</sup> where the mixture was left to react overnight and the dioxane added two hours before workup. Precatalyst **1** was prepared according to a literature procedure.<sup>2</sup> Silica gel (high-purity, 35-60 mesh, pore size 150 Å, BET surface area 300 m<sup>2</sup>/g) was purchased from Sigma-Aldrich and prepared as described below. <sup>57</sup>Fe (Handelsvertreter Cyclotron Instruments, Germany) and FeCl<sub>3</sub> (Aldrich, sublimed grade) were used as received.

**Physical and Analytical Measurements.** Solution NMR experiments were conducted using a Bruker UltraShield 500 MHz spectrometer (<sup>1</sup>H = 500 MHz, <sup>13</sup>C = 125 MHz) and the spectra were analyzed using MNova (v111, Mestrelab Research S.L, Spain). Chemical shifts for <sup>1</sup>H spectra were referenced using internal protio-solvent resonances and are reported relative to tetramethylsilane (TMS). Elemental analyses (Fe, C, H) were conducted by Galbraith Laboratories, Inc. (Knoxville, TN). Diffuse Reflectance Infrared Fourier Transform Spectroscopy (DRIFTS) spectra were acquired using Thermo Scientific™ Nicolet iS50 FT-IR Spectrometer equipped with an iS50 Automated Beamsplitter exchanger (ABX). The Praying Mantis™ accessory was used to collect the spectra of the samples under air-free and moisture-free conditions. The samples were prepared inside the glove box and placed on the sample cup of the high temperature reaction chamber, which includes ZnSe windows. The reaction chamber was then sealed and transferred to the FT-IR spectrometer. The measurements were made using a MCT/A detector without flowing any gases through the reaction chamber. A dried KBr spectrum was used as a background. The UV-Vis spectra were obtained on a Shimadzu UV-3600 Plus spectrometer equipped with a PMT (photomultiplier tube) detector. Similar to the DRIFTS experiment, sample preparation was conducted inside the glove box. The sample was diluted with polytetrafluoroethylene (PTFE) and tightly packed in the sample cup of the Praying Mantis™

reaction cell and then transferred to the spectrophotometer. The reflectance from the sample was measured from 200 to 800 nm at a medium scan speed with a sampling interval of 1 nm and a slit width of 3 nm. A background spectrum was obtained using the respective SiO<sub>2</sub> and was subtracted from the sample spectrum. A JEOL JEM-2100F transmission electron microscope (TEM) was used for all bright field imaging at 200 kV. Samples were prepared by dispersing solids in ethanol via sonication outside of a glovebox for 30 s. Colloidal suspensions were drop cast onto lacey C on Cu grids (300 mesh) from Electron Microscopy Sciences. Near IR Raman spectra were obtained using a Renishaw InVia Raman microscope through a 20x objective lens of a microscope with an excitation laser wavelength of 785 nm. All iron compounds were mounted into glass capillaries and epoxy-sealed in a N<sub>2</sub> glovebox prior to the Raman measurements. The laser power at the sample was kept very low (~3 mW), 1% of the full laser power. All Raman spectra were recorded at room temperature. The Mössbauer spectroscopy measurements were performed using a standard constant acceleration spectrometer. The source was a <sup>57</sup>Co/Pd point source with an activity level of about 1 mCi. Self-absorption in the source caused the line width to be broad, around 0.4 mm/sec, when measured with a stainless steel absorber. The detector used was a solid state VORTEX detector with excellent energy resolution of about 150 eV at 14.4 keV. The <sup>57</sup>Fe enriched samples were sealed with Kapton tape, which minimized oxidation. Data analysis was done using the CONUSS program.<sup>2</sup>

## **EPR Analysis**

Continuous-wave (CW) X-band (9-10 GHz) EPR experiments were carried out with a Bruker ELEXSYS II E500 EPR spectrometer (Bruker Biospin, Rheinstetten, Germany), equipped with a TE<sub>102</sub> rectangular EPR resonator (Bruker ER 4102ST). Data processing was done using Xepr (Bruker BioSpin) and Matlab 7.11.2 (The MathWorks, Inc., Natick). Compounds **1** and **2** were examined by EPR spectroscopy at low temperature to probe the iron oxidation states after grafting. Initially, compound **2** was analyzed as-prepared (2% Fe wt. loading). This resulted in a broad EPR spectra consistent with high-spin Fe(II). Since the broadness of the signal may be due to exchanged-coupled species, further analysis was performed on material loaded at 0.1% Fe. This material also gave a broad EPR signal, which was similar to the original 2% sample after normalization of the signal intensity, Figure S3. As such, compound **1** was only analyzed at the 0.1% Fe loading, and also produced a broad signal, much like that of **2**. Small signals for Fe(III)

were also detected in both **1** and **2**; however, these were due to trace Fe(III) impurities in the silica. Spectral subtraction of the silica supports from the prepared catalysts yields clean spectra with no traces of Fe(III), Figure S4. Upon exposure to air, **1** and **2** rapidly turn dark in color. EPR analysis reveals complete oxidation to high-spin Fe(III) species, Figures S5 and S6. EPR data were also collected on  $[\text{Fe}(\mu\text{-Mes})\text{Mes}]_2$  for comparison and this compound was found to be EPR silent under the same conditions, likely due to antiferromagnetic coupling between the metal centers.

### Catalyst Synthesis

**SiO<sub>2-200</sub>**. Silica gel (Aldrich, high-purity, 35-60 mesh, pore size 150 Å, BET surface area 300 m<sup>2</sup>/g) was heated to 200 °C and held at this temperature for 12 h under reduced pressure (15 mtorr). After activation, the sample was stored in a glovebox.

**SiO<sub>2-700</sub>**. Silica gel (Aldrich, high-purity, 35-60 mesh, pore size 150 Å, BET surface area 300 m<sup>2</sup>/g) was heated to 700 °C (temperature ramped over 2.25 h) and held at this temperature for 12 h under reduced pressure (15 mtorr). After activation, the sample was stored in a glovebox.

**FeSiO<sub>2-700</sub>, 1**. This preparation was adapted from a literature procedure.<sup>3</sup> SiO<sub>2-700</sub> (1.265 g) was added to a scintillation vial containing toluene (10 mL) and a stir bar.  $[\text{Fe}(\mu\text{-Mes})\text{Mes}]_2$  (147 mg) was dissolved in toluene (10 mL) in a second scintillation vial to form a red solution. Both vials were chilled to -30 °C and the  $[\text{Fe}(\mu\text{-Mes})\text{Mes}]_2$  solution was added to the SiO<sub>2-700</sub> slurry with stirring. The slurry was stirred for 1 h at -30 °C and then held at this temperature for 12 h. The toluene was then decanted, and the solids washed three times with toluene (10 mL each) and three times with pentane (10 mL each). The solids were then stirred in pentane for 30 min, the pentane decanted, and the solids dried thoroughly under reduced pressure to yield FeSiO<sub>2-700</sub>, **1**. Elemental Analysis found: Fe, 1.73%; C, 5.63%.

**FeSiO<sub>2-200</sub>, 2**. SiO<sub>2-200</sub> (5.001 g) was added to a 100 mL round bottom flask containing toluene (30 mL) and a stir bar.  $[\text{Fe}(\mu\text{-Mes})\text{Mes}]_2$  (523 mg) was dissolved in toluene (20 mL) and added dropwise over 5 min to the stirring SiO<sub>2-200</sub> slurry. The mixture was allowed to stir at room temperature for 1.5 h. The toluene was then decanted and the solids washed three times with toluene (20 mL each) and three times with pentane (20 mL each). The solids were then stirred in pentane for 30 min, the pentane decanted, and the solids dried thoroughly under reduced pressure to yield FeSiO<sub>2-200</sub>, **2**. Elemental Analysis found: Fe, 1.52%; C, 2.38%.

## NMR grafting experiments.

(Representative procedure) SiO<sub>2-200</sub> (193 mg) and [Fe( $\mu$ -Mes)Mes]<sub>2</sub> (19.8 mg) were combined with an internal standard, 1,3,5-tri-tert-butylbenzene (12.0 mg), in a 1.5 dram vial containing a stir bar. C<sub>6</sub>D<sub>6</sub> (1.5 mL) was added and the mixture stirred for 1.5 h. The solution was filtered into an NMR tube and the NMR spectrum used to quantitate the mesitylene released upon grafting. 2.1 moles mesitylene were found to be liberated per mol [Fe( $\mu$ -Mes)Mes]<sub>2</sub>.

(Representative procedure) SiO<sub>2-700</sub> (204 mg) and [Fe( $\mu$ -Mes)Mes]<sub>2</sub> (21.6 mg) were combined with an internal standard, 1,3,5-tri-tert-butylbenzene (12.6 mg), in a 1.5 dram vial containing a stir bar and chilled to -30 °C. Toluene-d<sub>8</sub> (1.5 mL) was chilled to -30 °C in a separate 1.5 dram vial and added to the vial containing the solids. The slurry was stirred at -30 °C for 2 h and left to stand at this temperature for 12 h. The solution was filtered into an NMR tube and the NMR spectrum used to quantitate the mesitylene released upon grafting. One mole mesitylene was found to be liberated per mole [Fe( $\mu$ -Mes)Mes]<sub>2</sub>.

## Preparation of <sup>57</sup>Fe-labeled catalysts

<sup>57</sup>Fe-labeled FeCl<sub>2</sub>·THF<sub>1.5</sub> was prepared by a modified combination of literature procedures.<sup>4,5</sup> <sup>57</sup>Fe metal (127 mg, 2.27 mmol) was cut into small pieces (ca. 0.5 mm x 2 mm) and added to a 100 mL Schlenk flask containing a magnetic stir bar. Solid FeCl<sub>3</sub> (735 mg, 4.53 mmol) and THF (50 mL) were then added to the flask to form a pale greenish-yellow solution. The flask was removed from the glovebox and refluxed under N<sub>2</sub> for 7 d during which time a fine pale precipitate formed. The flask was brought back into a N<sub>2</sub>-containing glovebox and the solids filtered on a medium frit. The remaining <sup>57</sup>Fe was still attached to the stir bar and removed. The solids were washed with THF (3x10 mL) to remove excess FeCl<sub>3</sub>, then with pentane (3x10 mL), and dried under reduced pressure to yield off-white solids (898 mg, 56%). This material was then used to make [Fe( $\mu$ -Mes)Mes]<sub>2</sub>, **1**, and **2**, in the same manner as described above.

## X-ray Absorption Experiments

X-ray absorption near edge structure (XANES) and extended X-ray absorption fine structure (EXAFS) measurements were carried out at the bending-magnet beamline of the Materials Research Collaborative Access Team (MR-CAT/10BM) at Argonne National Laboratory's Advanced Photon Source. All XAFS measurements were taken in the fluorescence mode with a

four element Vortex®-ME4 X-ray detector. A Fe metal foil to calibrate the K edge energy to 7110.75 eV for the zero-crossing in the second derivative. The sample was packed in Kapton® capillaries with both ends sealed by epoxy resin and moved to the sample holder within the closed cycle cryocooler (Advanced Research Systems) vacuum chamber. The sample was cooled down to lower than 25K to avoid photo degradation. The Si(111) double-crystal monochromator was detuned to 50% of the maximum intensity to reduce harmonics. Data were processed and analyzed using the Athena/Artemis software suite (version 0.26).<sup>6</sup>

## Catalyst Testing

Note: rigorous exclusion of air and moisture is necessary in these experiments as the catalysts are extremely sensitive to both.

Hydrogenation of 1-octene and cyclohexene was conducted using the Optimization Screening Reactor (OSR, Unchained Labs Inc.) located in a N<sub>2</sub>-filled glovebox (MB 200B, MBraun) in Argonne National Laboratory's High-throughput Research Facility. It has 8 parallel batch reactors with independent temperature and pressure controls and a common overhead stirring mechanism. It also has the capability of sampling and injection during reaction as well as monitoring the gas uptake. First, FeSiO<sub>2-700</sub>, **1**, or Fe/SiO<sub>2-700</sub>, **2**, (50 mg for 1-octene experiments, 100 mg for cyclohexene experiments) were loaded manually. Then, 25 mL of stock solution (0.25 M 1-octene or cyclohexene in dodecane) was added manually. The rest of the procedure was controlled by the LEA software; the reactors were purged with N<sub>2</sub> twice at 25 °C, flushed twice and pressurized with H<sub>2</sub> (UHP grade, oxygen and moisture trapped) up to 200 psi-g. Stirring was set at 700 rpm.

In the case of 1-octene, due to isomerization, sampling of aliquots was needed, so a settling delay was set at 15 sec prior to sampling to avoid carrying over catalyst powder. Trimethoxybenzene was used as an internal standard. Automated sampling of 100 µL was performed at various times, and dispensed into filter vials (Whatman Mini-UniPrep Syringeless Filter, 0.2 µm) preloaded with 100 µL of dodecane, on 48 well plates, located on the automated platform deck (Core Module CM3, Unchained Labs Inc.). For cyclohexene, there was no settling delay and hydrogen uptake was measured instead. This allows for the generation of many more data points and also eliminates the need to stop stirring during sampling, which can affect the perceived catalytic rates.

## GC-MS and GC-FID Analysis

The compositions of the reaction mixtures were determined using a Trace GC Ultra Gas Chromatograph system equipped with a Tri Plus RSH autosampler, an ISQ MS detector, and a FID (Thermo Scientific). The column used for the MS detector was an Agilent J&W DB-5 column (30 m × 0.25 mm × 0.25 μm film thickness), while the column used for the FID was an Agilent J&W DB-5MS column (30 m × 0.25 mm × 0.25 μm film thickness). GC data were analyzed using the Thermo Xcalibur 2.2 SP1.48 software. The following method was used: a 0.5 μL split injection with a split ratio of 100 was run under a constant gas flow of 1 mL/min. The oven temperature profile was as follows: initial temperature = 28 °C, hold for 10 minutes, ramp at 20 °C/min, final temperature = 250 °C.

**Table 1.** Observed and calculated (DFT) frequencies (cm<sup>-1</sup>) in the 200-1300 cm<sup>-1</sup> region of the Raman spectra of mesitylene, [Fe(μ-Mes)Mes]<sub>2</sub>, **1**, and **2**, along with the vibrational assignments. DFT vibrational frequencies are multiplied by a vibrational scale factor of 0.9657 based on the benchmark for B3LYP/CEP-31G.<sup>7</sup> Assignment: ν: stretching, δ: in-plane bending, γ: out-of-plane bending, τ: torsion, Γ: rocking.<sup>8</sup>

Mesitylene		[Fe(μ-Mes)Mes] <sub>2</sub>		1		2		Assignment
Obs.	DFT	Obs.	DFT	Obs.	DFT	Obs.	DFT	
233	222	222	226	215	211	--	231	γ(CH) [τ(CCCC) + τ(CCCH)]
279	255	285	286	280 (VW)	282	278	276	δ(CC-CH <sub>3</sub> ) + δ(Fe-CC)
519	509	533	529	534	533	533	533	δ(CCC) + ν(CC) + δ(CC-CH <sub>3</sub> )
--	--	558	550	562	550	--	--	ν(Fe-C-Fe)
580	549	578, 582	556	575, 581	557	576	552	ν(C-CH <sub>3</sub> ) + ν(CC)
--	--	938 (VW)	914	939 (VW)	970	--	--	ν(Fe-C-Fe)
1001	1001	1002	1003	1005	1011	1002	1002	ν(CC) + δ(CCC)
1043	1041	1028, 1051 (VW)	1014, 1039	1027	1026	--	1009	Γ(CH <sub>3</sub> ) [δ(CCH)] + τ(CCCH)

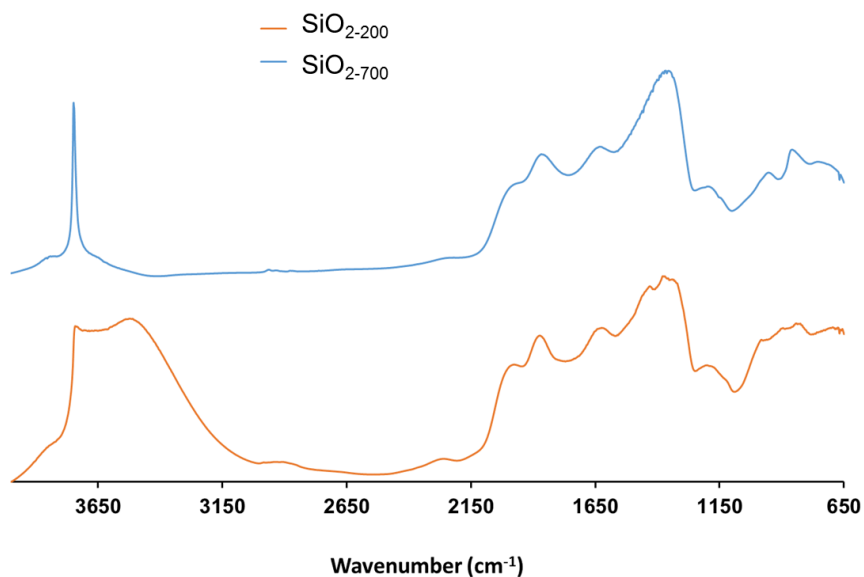


**Figure S1.** DRIFTS analysis of SiO<sub>2-700</sub>, **1** (top) and SiO<sub>2-200</sub>, **2** (bottom). The sharp peak at 3750 cm<sup>-1</sup> is indicative of isolated silanols, while the broad feature from 3100–3650 cm<sup>-1</sup> corresponds to vicinal silanols that are removed at higher temperatures.

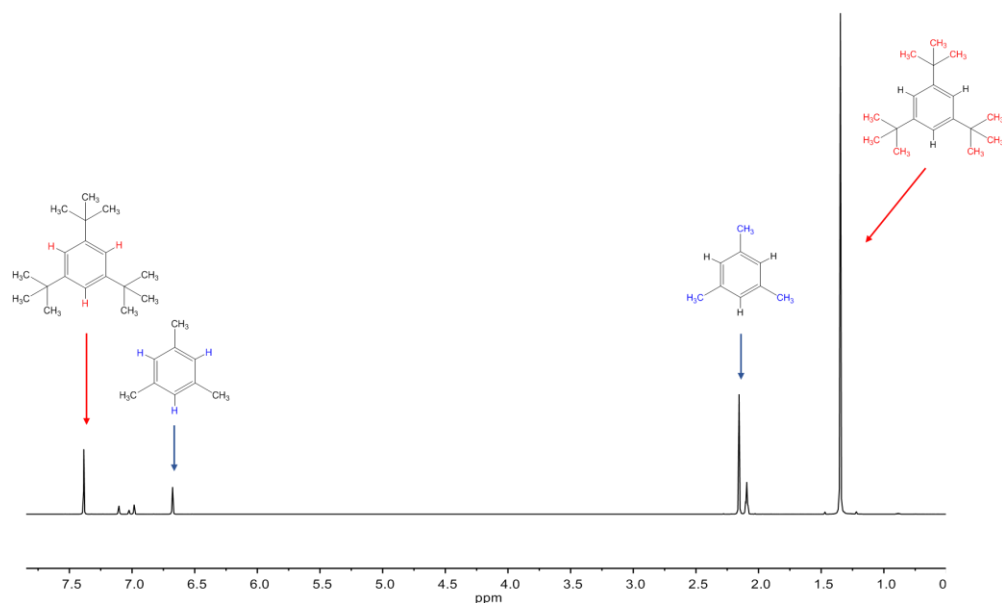


**Figure S2.** An example NMR spectrum in toluene-d<sub>8</sub> from the grafting experiments showing resonances for liberated mesitylene and the 1,3,5-tri-tertbutyl benzene internal standard.

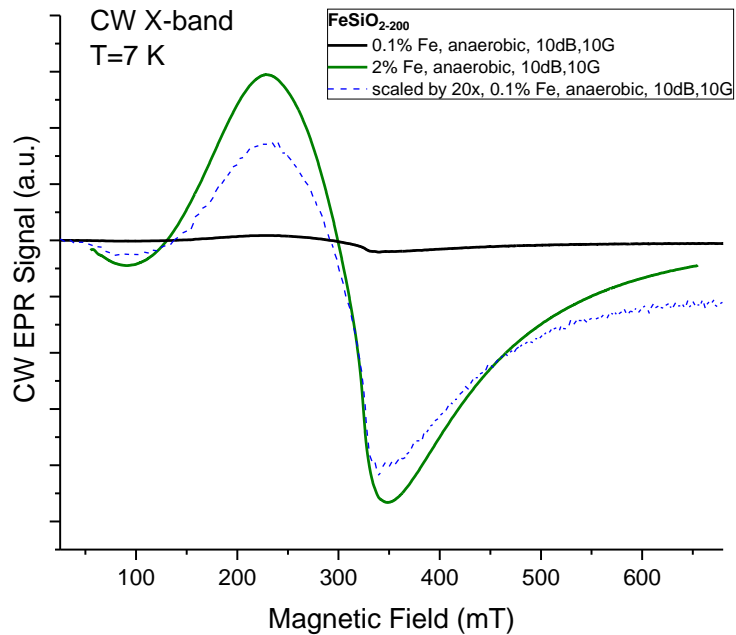


**Figure S3.** Comparison of EPR spectra from  $\text{FeSiO}_{2-200}$ , **2**, prepared at 2% Fe (green solid line), 0.1% Fe (black solid line), and 0.1% Fe magnified 20x (blue dashed line).

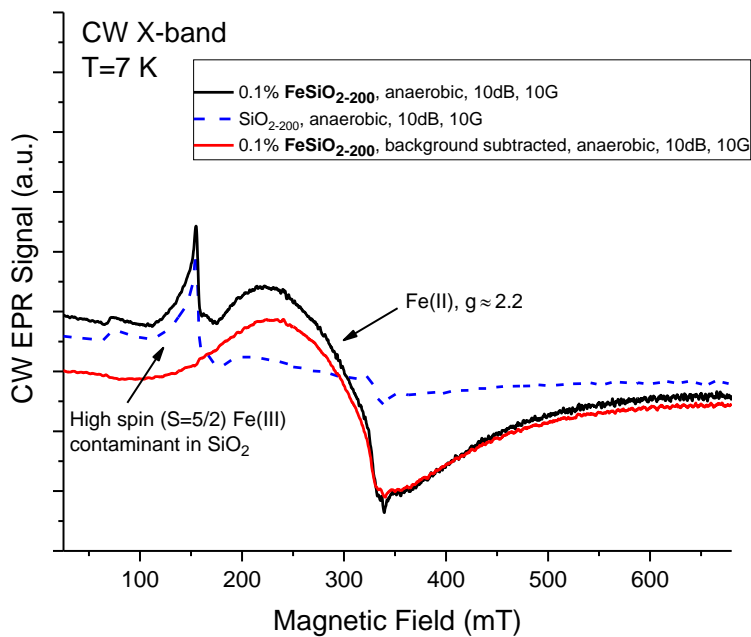


**Figure S4.** EPR spectra for  $\text{FeSiO}_{2-200}$ , **2**, prepared at 0.1% Fe (black solid line),  $\text{SiO}_{2-200}$  background (blue dashed line), and resulting background subtracted spectra (red solid line).

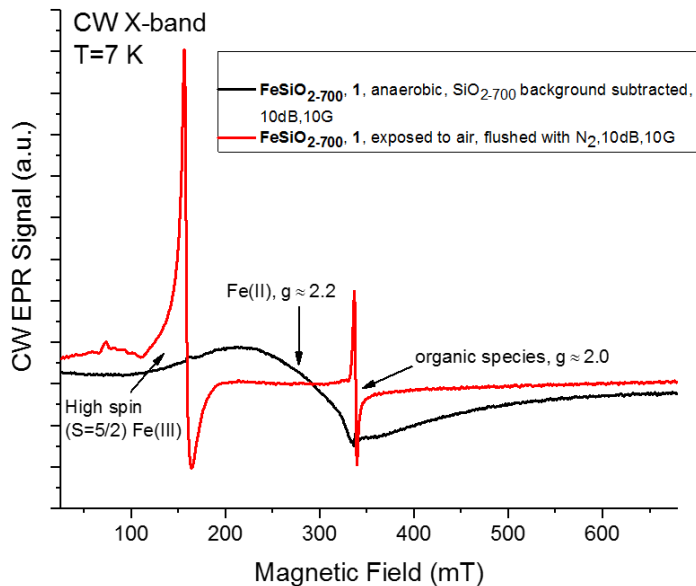


**Figure S5.** EPR spectra for  $\text{FeSiO}_{2-700}$ , **1**, as prepared, background subtracted, showing Fe(II) surface sites (black) which oxidize to Fe(III) upon exposure to air (red). Organic radicals were also observed at  $g = 2.0$  in the oxidized sample.

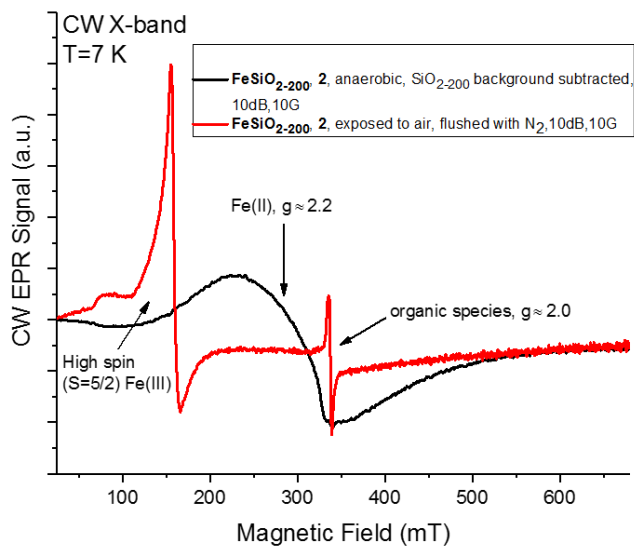


**Figure S6.** EPR spectra for  $\text{FeSiO}_{2-200}$ , **2**, as prepared, background subtracted, showing Fe(II) surface sites (black) which oxidize to Fe(III) upon exposure to air (red). Organic radicals were also observed at  $g = 2.0$  in the oxidized sample.

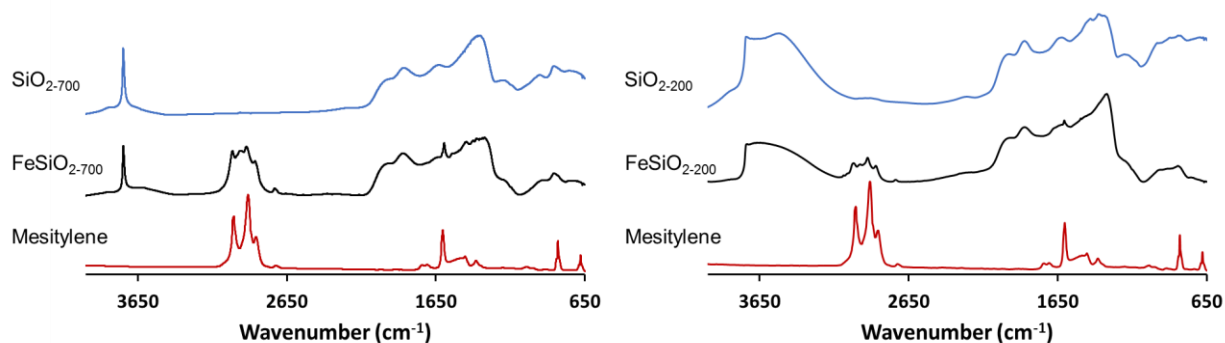


**Figure S7.** Diffuse Reflectance Infrared Fourier Transform Spectroscopy (DRIFTS) spectra showing incorporation of mesitylene functionality on the SiO<sub>2</sub> surface.

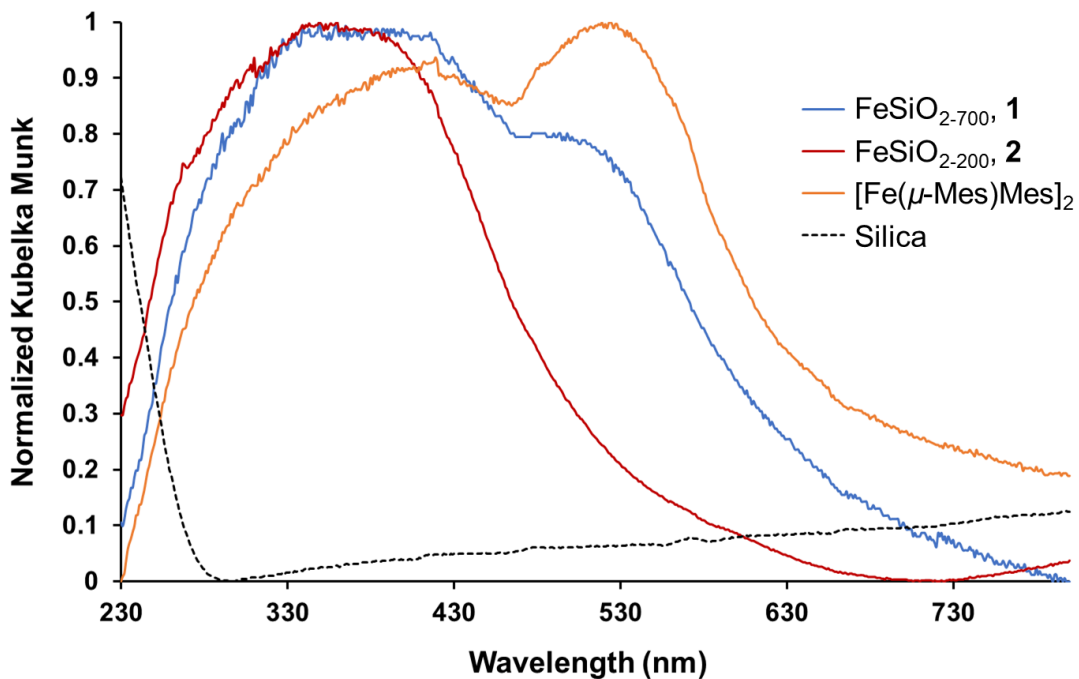


**Figure S8.** Diffuse Reflectance Ultraviolet-Visible (DRUV) spectra of **1** (blue), **2** (red), [Fe( $\mu$ -Mes)Mes]<sub>2</sub> (orange), and SiO<sub>2</sub> (black dashed).

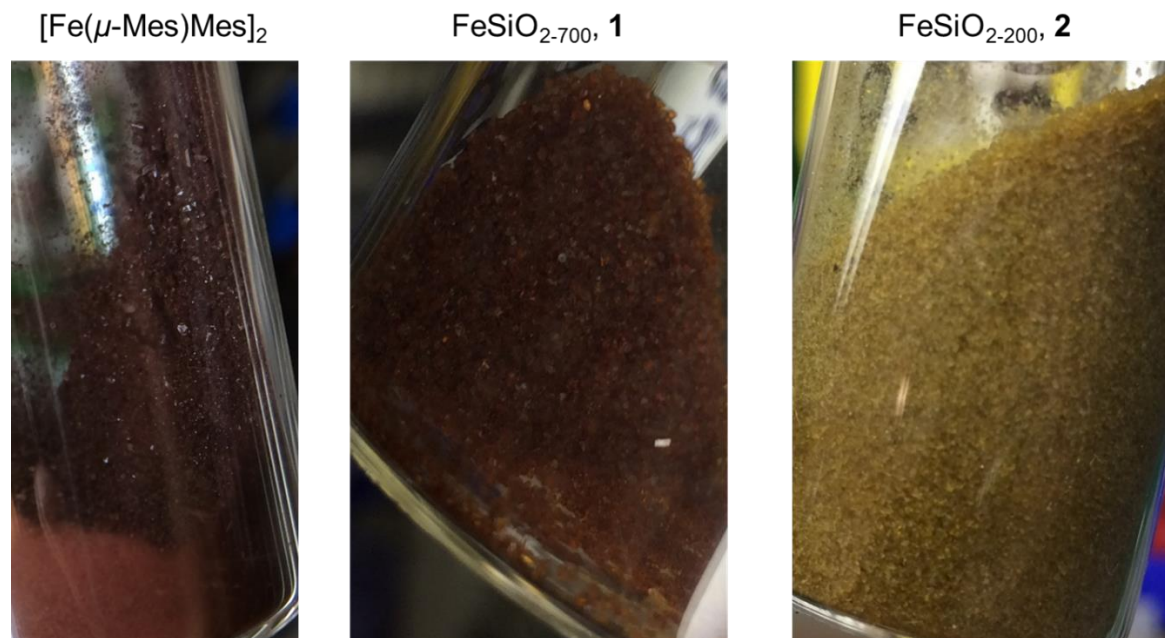


**Figure S9.** Appearance of  $[\text{Fe}(\mu\text{-Mes})\text{Mes}]_2$  (left),  $\text{FeSiO}_{2-700}$ , **1**, (middle), and  $\text{FeSiO}_{2-200}$ , **2**, (right).

## Computational Details

### Models and Methods

Two cluster models of silica with silsesquioxane cages,  $\text{SiO}_{2-200}$  (Figure S10a) and  $\text{SiO}_{2-700}$  (Figure S10b), were used to model  $\text{FeSiO}_{2-200}$ , **2**, and  $\text{SiO}_{2-700}$ , **1**, respectively. Previous studies have shown that silsesquioxane cages are good representations for amorphous silica.<sup>9</sup> The cluster model in Figure S10(a) was developed in our recent computational study of silica-supported metal ions.<sup>10</sup> This model contains six silica rings, four hydroxyls and the corner Si atoms were terminated with hydrogen atoms. It was previously shown to sufficiently reproduce the relative stability of the metal center species and the silica ring strain of the periodic model for silica.<sup>10</sup> This model is a good representation of  $\text{SiO}_{2-200}$ , where higher concentrations of the hydroxyls are present on the surface. On the other hand, we adopted the cluster model in Figure S10b for the calculations of  $\text{SiO}_{2-700}$ , where much lower concentrations of the hydroxyls are present on the surface. This model only contains one hydroxyl group.

All the calculations were carried out using B3LYP functional<sup>11,12</sup> with a CEP-31G<sup>13-15</sup> basis set as available for the E.01 version of the Gaussian09 program.<sup>16</sup> The bottom half of the clusters

were kept frozen during the calculations while the top half and the interacting molecules were allowed to relax.

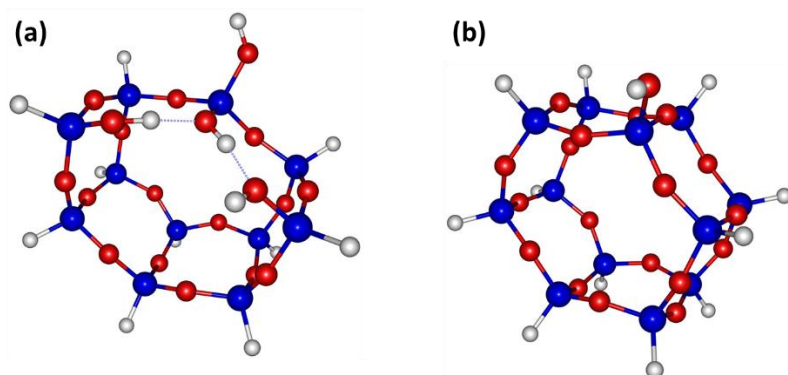


**Figure S10.** Cluster models of (a)  $\text{SiO}_2\text{-200}$  and (b)  $\text{SiO}_2\text{-700}$ .

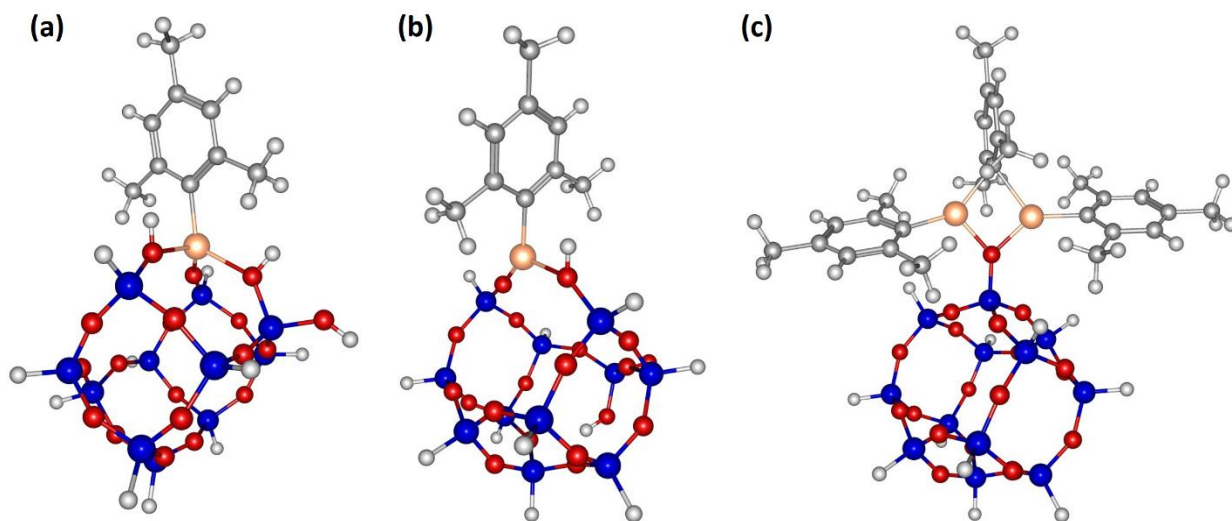
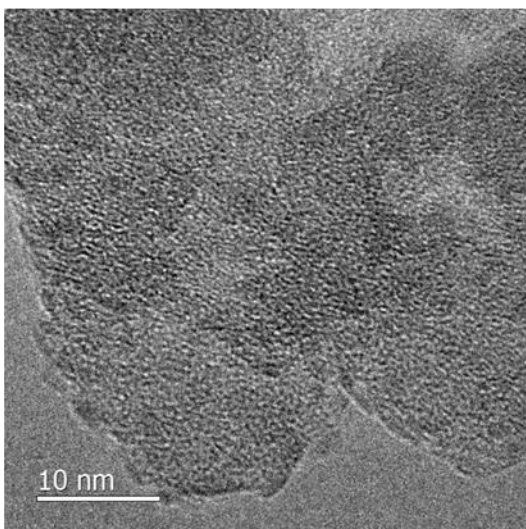


**Figure S11.** Optimized structures of a) 4-coordinate **2**, b) 3-coordinate **2**, and c) **1**.

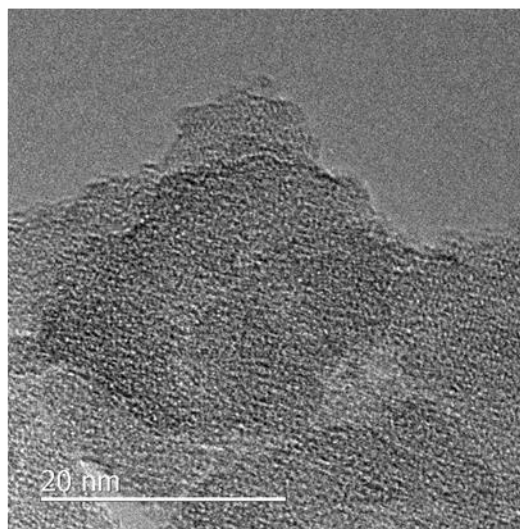
#### xyz coordinates of optimized Fe systems

For xyz coordinates, see .xyz file uploaded as Supporting Information.

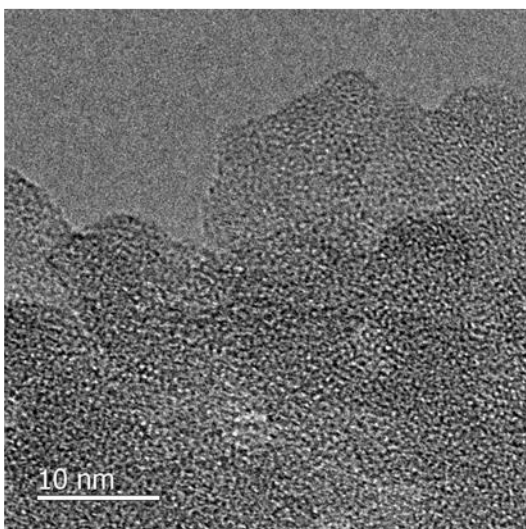
a)  $\text{FeSiO}_{2-700}$ , **1**, as prepared



b)  $\text{FeSiO}_{2-700}$ , **1**, Post  $\text{H}_2$



c)  $\text{FeSiO}_{2-200}$ , **2**, as prepared



d)  $\text{FeSiO}_{2-200}$ , **2**, Post  $\text{H}_2$

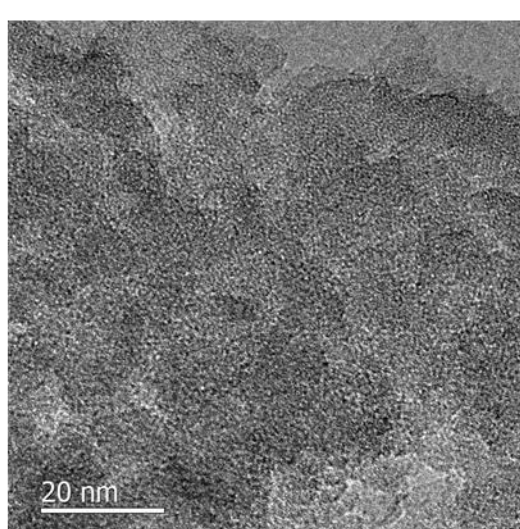


**Figure S12.** TEM images of a) **1**, as prepared; b) **1** after treatment with  $\text{H}_2$  at  $180\text{ }^\circ\text{C}$  for 30 min; c) **2** as prepared; and d) **2** after treatment with  $\text{H}_2$  at  $180\text{ }^\circ\text{C}$  for 30 min.

### Detection Limits for Fe metal nanoparticles

XAFS measurements were made to determine the Fe environment in the catalysts, Figure S13 The XANES region for Fe on FeSiO<sub>2-700</sub>, **1**, + H<sub>2</sub> exhibits a feature at ~7712 eV that could be due to metallic Fe, although it is worth noting that [Fe( $\mu$ -Mes)Mes]<sub>2</sub> also exhibits increased intensity in this region. Therefore, this feature alone is not an indicator of metallic iron. Figure S14 shows the Fourier transform magnitude. Observe the higher-R scattering path region between 4 Å and 5 Å. Even though the Fe metal foil spectrum has been multiplied by 0.2, the amplitude is much greater than the two unknown samples. This severely limits the Fe metal nanoparticle amount. Also note that the FeSiO<sub>2-700</sub>, **1**, + H<sub>2</sub> was measured below 20K, which would substantially enhance a metallic higher-shell scattering path signal. Based on these observations, the fraction of Fe in metallic nanoparticles must be less than 5%.

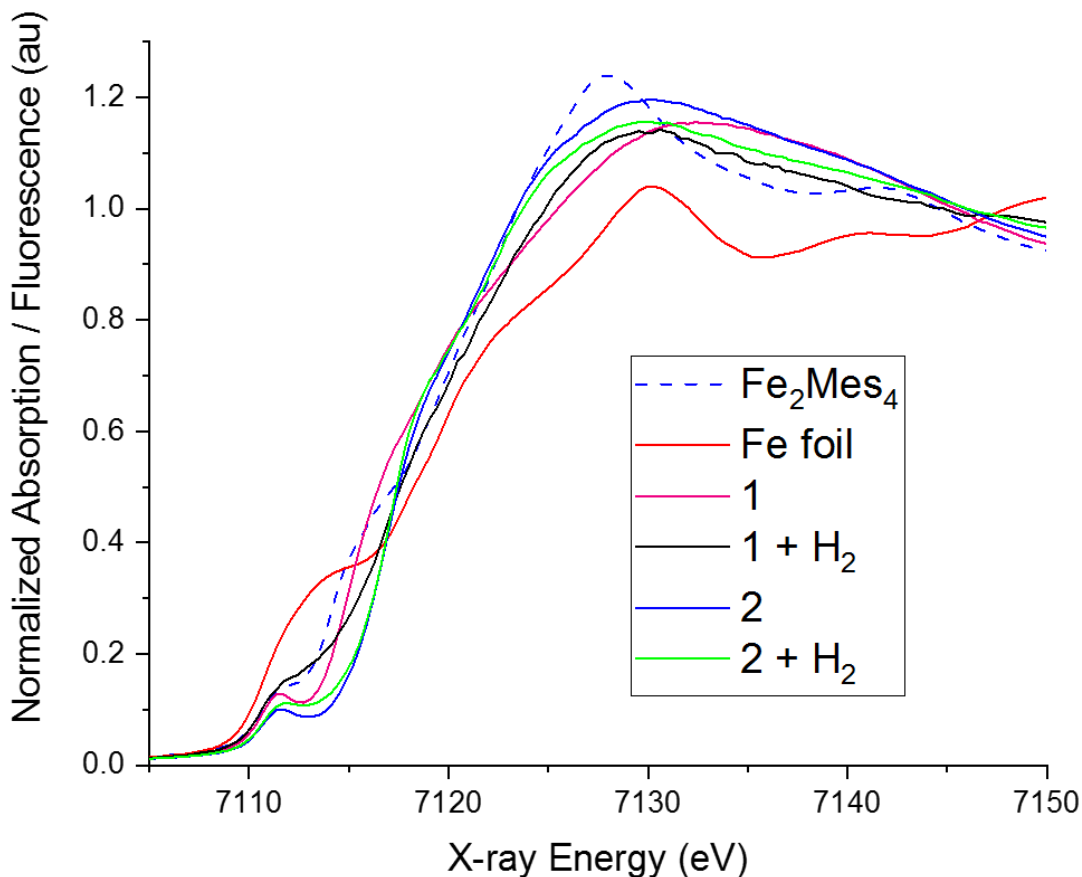


**Figure S13.** Fe K edge XANES.

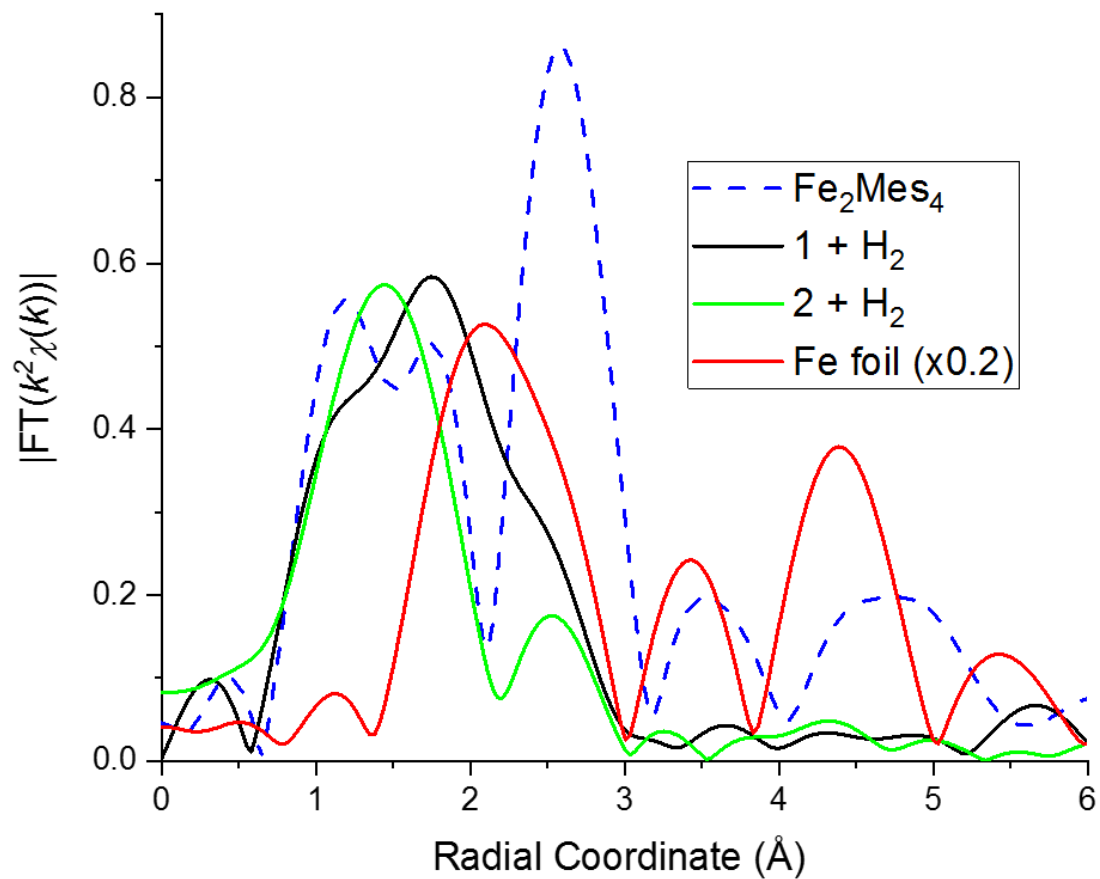


**Figure S14.** Magnitude of the  $k^2$ -weighted Fourier transform from  $3 \text{ \AA}^{-1} < k < 8.5 \text{ \AA}^{-1}$ . Fe metal foil is multiplied by 0.2 to fit on the same scale.

## References

1. A. Klose, E. Solari, C. Floriani, A. Chiesi-Villa, C. Rizzoli and N. Re, *Journal of the American Chemical Society*, 1994, **116**, 9123-9135.
2. W. Sturhahn, *Hyperfine Interactions* 2000, **125**, 149-172.
3. C. Roukoss, J.-M. Basset, C. Copéret, C. Lucas and E. Kuntz, *Comptes Rendus Chimie*, 2008, **11**, 620-627.
4. G. Wilkinson, *Org. Synth.*, 1956, **36**, 31-35.
5. C.-L. Sun, H. Krause and A. Fürstner, *Advanced Synthesis & Catalysis*, 2014, **356**, 1281-1291.
6. Ravel, B.; Newville, M., *J Synchrotron Radiat* 2005, **12**, 537-541.
7. NIST Computational Chemistry Comparison and Benchmark Database. NIST Standard Reference Database Number 101. Release 18, October 2016, Editor: Russell D. Johnson III. <http://cccbdb.nist.gov/>.
8. E. Kose, A. Atac, M. Karabacak, P. B. Nagabalasubramanian, A. M. Asiri and S. Periandy, *Spectrochim. Acta, Part A*, 2013, **116**, 622-634.
9. F. J. Feher, D. A. Newman, J. F. Walzer, *Journal of the American Chemical Society* 1989, **111**, 1741-1748.
10. U. Das, G. Zhang, B. Hu, A. S. Hock, P. C. Redfern, J. T. Miller, L. A. Curtiss, *ACS Catalysis* 2015, **5**, 7177-7185.
11. A. D. Becke, *The Journal of Chemical Physics* 1993, **98**, 5648-5652.
12. C. Lee, W. Yang, R. G. Parr, *Physical Review B* 1988, **37**, 785-789.
13. W. J. Stevens, H. Basch, M. Krauss, *The Journal of Chemical Physics* 1984, **81**, 6026-6033.
14. W. J. Stevens, M. Krauss, H. Basch, P. G. Jasien, *Canadian Journal of Chemistry* 1992, **70**, 612-630.
15. T. R. Cundari, W. J. Stevens, *The Journal of Chemical Physics* **1993**, **98**, 5555-5565.
16. M. J. Frisch, G. W. Trucks, H. B. Schlegel, G. E. Scuseria, M. A. Robb, J. R. Cheeseman, G. Scalmani, V. Barone, B. Mennucci, G. A. Petersson, H. Nakatsuji, M. Caricato, X. Li, H. P. Hratchian, A. F. Izmaylov, J. Bloino, G. Zheng, J. L. Sonnenberg, M. Hada, M. Ehara, K. Toyota, R. Fukuda, J. Hasegawa, M. Ishida, T. Nakajima, Y. Honda, O. Kitao, H. Nakai, T. Vreven, J. A. Montgomery Jr., J. E. Peralta, F. Ogliaro, M. J. Bearpark, J. Heyd, E. N. Brothers, K. N. Kudin, V. N. Staroverov, R. Kobayashi, J. Normand, K. Raghavachari, A. P. Rendell, J. C. Burant, S. S. Iyengar, J. Tomasi, M. Cossi, N. Rega, N. J. Millam, M. Klene, J. E. Knox, J. B. Cross, V. Bakken, C. Adamo, J. Jaramillo, R. Gomperts, R. E. Stratmann, O. Yazyev, A. J. Austin, R. Cammi, C. Pomelli, J. W. Ochterski, R. L. Martin, K. Morokuma, V. G. Zakrzewski, G. A. Voth, P. Salvador, J. J. Dannenberg, S. Dapprich, A. D. Daniels, Ö. Farkas, J. B. Foresman, J. V. Ortiz, J. Cioslowski, D. J. Fox, Gaussian, Inc., Wallingford, CT, USA, 2009.